Supporting Information

Highly controllable protein self-assembly system with morphological versatility induced by reengineered host-guest interaction

Xiumei Li, Yushi Bai, Zupeng Huang, Chengye Si, Zeyuan Dong, Quan Luo and Junqiu Liu*

State Key laboratory of Supramolecular Structure and Materials, College of Chemistry, Jilin University, Changchun 130012, China

1. Synthesis of the Maleimide-Functionalized Phe-Gly-Gly (MIFGG)

1.1 General information. All the reactions were performed in oven-dried apparatus and preparation of the substrates was carried out under inert N_2 atmosphere in dry solvents. All the reagents were bought from commercial suppliers and used without further purification unless stated otherwise. All the water was purified by a Millipore water purification system. Thin layer chromatography (TLC) was performed using aluminum-backed sheets of silica gel and visualized under a UV lamp (254 nm). Column chromatography was performed with silica gel (200-300 mesh). ^{1}H NMR spectra were recorded with a Bruker AVANCE III 500 apparatus using a tetramethylsilane (TMS) proton signal as the internal standard. ESI-MS spectrometric analyses were performed at the Thermo Finnigan LCQ AD System.

1.2 Synthesis of Boc-Phe-Gly.

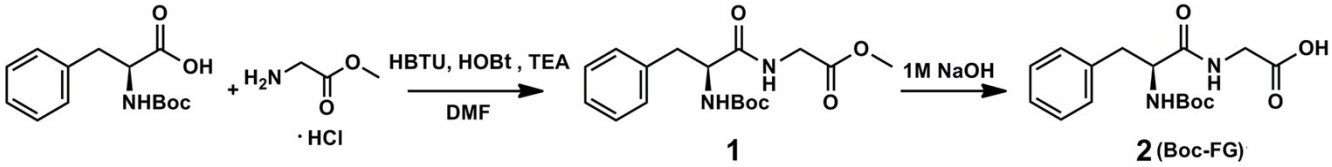

Scheme S1. Synthetic route of the BOC-FG.

A mixture of Boc-L-phenylalanine (2.65 g, 10 mmol), glycine methyl ester hydrochloride (891 mg, 10 mmol), 2-(1H-benzotriazole-1-yl)-1,1,3,3-tetramethylaminium hexafluorophosphate (HBTU) (3.79 g, 10 mmol) and 1-hydroxybenzotriazole (HOBt) (1.35 g, 10 mmol) was dissolved in 30 ml DMF. 4 ml TEA was added to the solution. The resulting solution was stirred at room temperature overnight and then evaporated to dryness. The crude product was purified by flash chromatography (dichloromethane/ethyl acetate=5/1) to yield the (S)-methyl 2-(2-((tert-butoxycarbonyl)amino)-3-phenylpropanamido)acetate (Boc-L-Phe-Gly-OMe) (product **1)** as a white solid (3.00 g, 90%). ^{1}H NMR (500 MHz, $CDCl_3$, 25 ^{o}C) δ(ppm): 7.30 (m, 2H), 7.22 (m, 3H), 6.35 (s, 1H), 4.95 (m, 1H), 4.40 (s, 1H), 4.02 (m, 2H), 3.74 (s, 3H), 3.10 (m, 2H), 1.40 (s, 9H).

Product **1** (1.682 g, 5 mmol) was dissolved in 10 mL of sodium hydroxide methanol solution (1 M). After stirring overnight, the mixture was evaporated under reduced pressure to dryness. The crude product was dissolved in water and acidified by HCl and extracted with ethyl acetate. The combined organic phase was dried over Na_2SO_4 and concentrated to yield the product **2** (Boc-FG) as white solid (1.56 g, 97%). ^{1}H NMR (500 MHz, DMSO-d_6, 25 ^{o}C) δ(ppm): 1.28 (m, 9H), 3.02 (m, 2H), 3.90 (m, 2H), 4.19 (m, 1H), 6.89 (m, 1H), 7.18 (m, 1H), 7.26 (m, 5H), 12.57 (m, 1H).

1.3 Synthesis of Furan-maleimide-Gly.

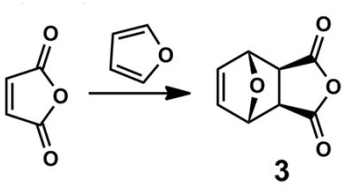

Scheme S2. Synthesis of the furan-protected maleic anhydride.

3a,4,7,7a-Tetrahydro-4,7-epoxyisobenzofuran-1,3-dione (Furan-protected maleic anhydride) (**3**) was synthesized according to a method reported by Haddleton et al.[1] Maleic anhydride (10.0 g, 102 mmol) was suspended in 50 mL of toluene and the mixture was heated to 80 °C. Furan (11.1 mL, 153 mmol) was added via syringe and the turbid solution was stirred for 6 h. The mixture was then cooled to room temperature and the stirring stopped. After 1 h, the resulting white crystals were collected by filtration and washed with petroleum ether. Product **3** was obtained as white crystal (14.4 g, 85%). ^{1}H NMR (500 MHz, $CDCl_3$, 25 ^{o}C) δ(ppm): 6.58 (s, 2H), 5.46 (s, 2H), 3.17 (s, 2H).

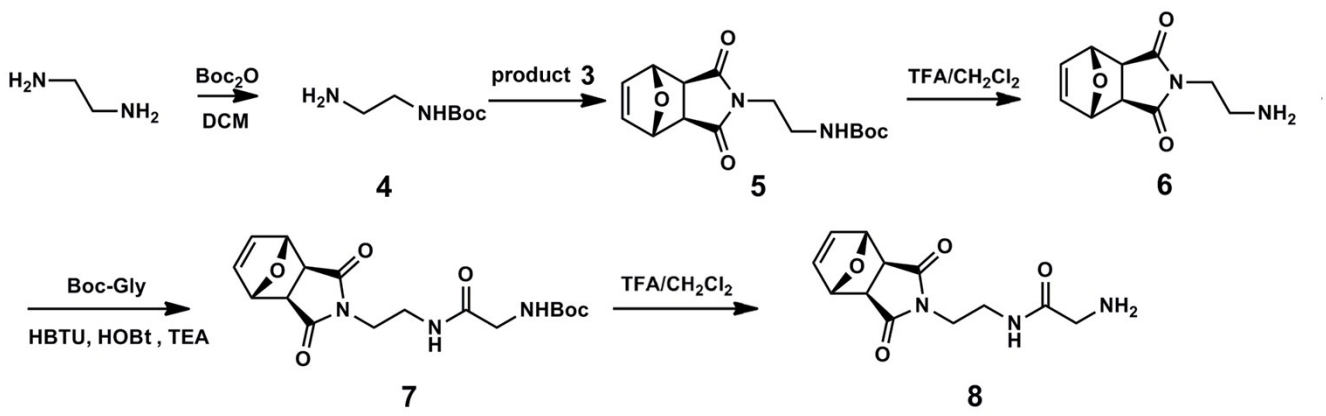

Scheme S3. Synthetic route of the furan-maleimide-Gly.

Tert-butyl *N*-(2-aminoethyl)carbamate (Boc-protected ethylenediamine) (**4**) was synthesized according to a method reported by Saari et al.[2] A solution of *ditert*-butyl dicarbonate (Boc_2O)(7.27 g, 33.3 mmol) in THF (30 mL) was added dropwise to a solution of ethylenediamine (6.7 mL, 100 mmol) in THF (30 mL) at 0 ^oC with stirring. The reaction mixture was stirred in an ice bath for 30 min after addition and further stirred at room temperature for 18 h. Solvents were removed under reduced pressure, and the residue was dissolved in water and extracted with ethyl acetate. The combined organic phase was dried over Na_2SO_4 and concentrated to yield the product **4** as colorless oil (5.00 g, 95%). ^1H NMR (500 MHz, $CDCl_3$, 25 ^oC) δ(ppm): 4.92 (s, 1H), 3.18 (m, 2H), 2.81 (t, J = 5.9 Hz, 2H), 1.74 (s, 2H), 1.44 (s, 9H).

Tert-butyl (2-((3aR,4S,7R,7aS)-1,3-dioxo-3a,4,7,7a-tetrahydro-1H-4,7-epoxyisoindol-2(3H)-yl)ethyl) carbamate (**5**) was synthesized according to an analogous strategy reported by Haddleton et al.[1] Furan-protected maleic anhydride (**3**) (8.30 g, 50 mmol) was suspended in MeOH (250 mL) and the mixture was cooled to 0 °C in ice bath. A solution of **4** (8.00 g, 50 mmol) in 100 mL of MeOH was added dropwise for 30 min with stirring at 0 °C, then the resulting mixture was stirred for 30 min at room temperature, and finally refluxed for 4 h. The solvent was removed under reduced pressure. The residue was dissolved in CH_2Cl_2 and washed with water. The organic layer was dried over Na_2SO_4 and filtered. The crude product was purified by flash chromatography (petroleum ether /ethyl acetate=5/1) to give **5** as a white solid (1.54 g, 10%). ^1H NMR (500 MHz, $CDCl_3$, 25 ^oC) δ(ppm): 6.52 (t, J = 0.8 Hz, 2H), 5.26 (s, 2H), 4.76 (s, 1H), 3.63 (t, 2H), 3.31 (m, 2H), 2.86 (s, 2H), 1.42 (s, 9H).

The cleavage of Boc was performed with a mixture of TFA and DCM (1:1 by volume). A solution of TFA/DCM (2 mL) was added dropwise into product **5 (**616.6 mg, 2 mmol) with stirring and further reacted at room temperature for 3 h. The solution was evaporated to give the (3aR,4S,7R,7aS)-2-(2-aminoethyl)-3a,4,7,7a-tetrahydro-1H-4,7-epoxyisoindole-1,3(2H)-dione (product **6**) as white solid (395 mg, 95%). ^{1}H NMR (500 MHz, DMSO-d_6, 25 ^{o}C) δ(ppm): 7.85 (s, 2H), 6.56 (s, 2H), 5.14 (s, 2H), 3.62 (t, J = 6.4 Hz, 2H), 3.05 – 2.78 (m, 4H).

A mixture of product **6** (350 mg, 1.68 mmol), Boc protected glycine (Boc-Gly) (270 mg, 1.68 mmol), 2-(1H-benzotriazole-1-yl)-1,1,3,3-tetramethylaminium hexafluorophosphate (HBTU) (637 mg, 1.68 mmol) and 1-hydroxybenzotriazole (HOBt) (227 mg, 1.68 mmol) was dissolved in 10 ml DMF. 0.8 ml TEA was added to the solution. The final solution after reaction was evaporated to dryness and the crude product was purified by flash chromatography (dichloromethane/ethyl acetate=4/1) to yield the tert-butyl (2-((2-((3aR,4S,7R,7aS)-1,3-dioxo-3a,4,7,7a-te/trahydro-1H-4,7-epoxyisoindol-2(3H)-yl)ethyl)amino)-2-oxoethyl)carbamate (product **7)** as a white solid (550 mg, 90%). ^{1}H NMR (500 MHz, CDCl3, 25 ^{o}C) δ(ppm): 6.51 (s, 2H), 5.28 (s, 2H), 3.74 (d, J = 5.8 Hz, 2H), 3.67 (dd, J = 6.4, 4.5 Hz, 2H), 3.49 (dd, J = 11.1, 5.7 Hz, 2H), 2.87 (s, 2H), 1.45 (s, 9H).

The cleavage of Boc was performed with a mixture of TFA and DCM (1:1 by volume). A solution of TFA/DCM (2 mL) was added dropwise into product **7 (**550 mg, 1.5 mmol) with stirring and further reacted at room temperature for 3 h. The final solution was evaporated to give the 2-amino-*N*-(2-((3aR,4S,7R,7aS)-1,3-dioxo-3a,4,7,7a-tetrahydro-1H-4,7-epoxyisoindol-2(3H)-yl)ethyl)acetamide (furan-maleimide-Gly) (product **8**) as white solid (367 mg, 92%). ^{1}H NMR (500 MHz, D_2O, 25 ^{o}C) δ(ppm): 6.63 (s, 2H), 5.31 (s, 2H), 3.67-3.70 (m, 4H), 3.50 (t, J = 5.7 Hz, 2H), 3.13 (s, 2H).

1.4 Linkage of the Boc-Phe-Gly and the Furan-maleimide-Gly to Synthesize the Final MIFGG.

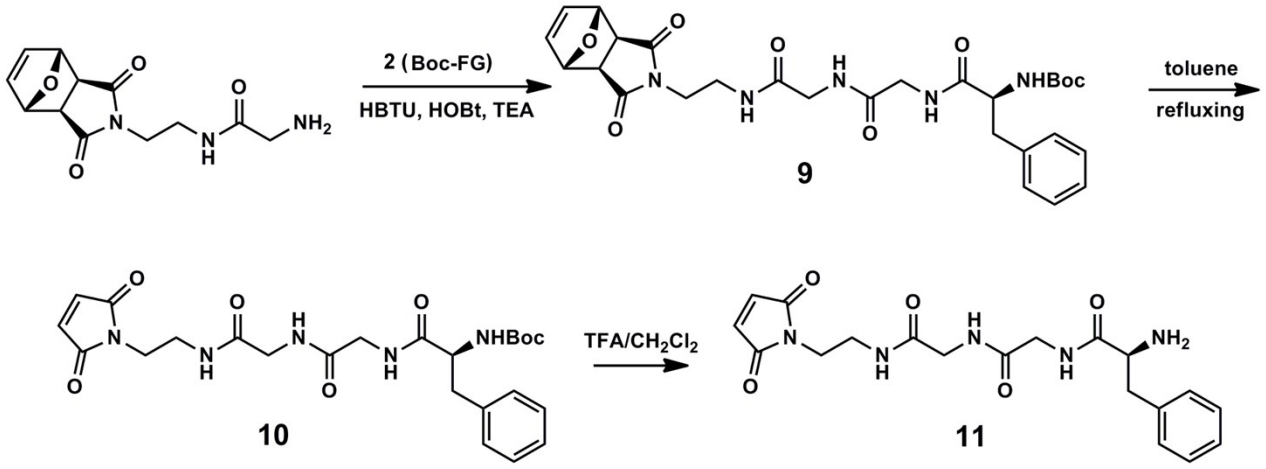

Scheme S4. Synthetic route of the maleimide-functionalized FGG.

A mixture of product **2** (Boc-FG) (420 mg, 1.3 mmol), product **8** (Furan-maleimide-Gly) (345 mg, 1.3 mmol), 2-(1H-benzotriazole-1-yl)-1,1,3,3-tetramethylaminium hexafluorophosphate (HBTU) (493 mg, 1.3 mmol) and 1-hydroxybenzotriazole (HOBt) (175 mg, 1.3 mmol) was dissolved in 6 ml DMF. 0.6 ml TEA was added to the solution. The final solution after reaction was evaporated to dryness and the crude product was purified by flash chromatography (dichloromethane/ethyl acetate=1/1) to yield the product **9** as yellow oil (680 mg, 92%). ^{1}H NMR (500 MHz, DMSO-d_6, 25 ^{o}C) δ(ppm): 8.21 (t, J = 5.4 Hz, 1H), 8.01 (s, 1H), 7.86 (s, 1H), 7.26 (d, J = 4.5 Hz, 4H), 7.19 (m, 1H), 7.00 (d, J = 8.5 Hz, 1H), 6.54 (s, 2H), 5.13 (s, 2H), 4.18 (s, 1H), 3.76 (d, J = 5.4 Hz, 2H), 3.63 (m, 2H), 3.42 (t, J = 6.6 Hz, 2H), 3.18 (dd, J = 12.8, 6.2 Hz, 2H), 2.92 (s, 2H), 1.29 (s, 9H).

The retro-Diels-Alder reaction was performed according to the method reported by Haddleton et al.[1] Product **9** (570 mg, 1 mmol) was suspended in toluene, and the mixture was heated to reflux with stirring for 6 h, the solvent was removed under reduced pressure to give product **10** as yellow oil (475 mg, 95%). ^{1}H NMR (500 MHz, CDCl3, 25 ^{o}C) δ(ppm): 7.40 – 7.30 (m, 2H), 7.32 – 7.27 (m, 1H), 7.21 (d, J = 7.0 Hz, 2H), 7.05 (s, 1H), 6.82 (s, 1H), 6.72 (s, 2H), 4.23 (d, J = 6.2 Hz, 1H), 4.04 (dd, J = 16.8, 6.5 Hz, 1H), 3.83 (dtd, J = 32.5, 16.6, 6.3 Hz, 3H), 3.44 (p, J = 14.4 Hz, 2H), 3.21 – 3.13 (m, 4H), 1.39 (s, 9H).

The cleavage of Boc was performed with a mixture of TFA and DCM (1:1 by volume). A solution of TFA/DCM (1.5 mL) was added dropwise into product **10 (**400 mg, 0.8 mmol) with stirring and further reacted at room temperature for 3 h. The final solution was evaporated to give the final 2-amino-*N*-(2-((2-((2-(2,5-dioxo-2,5-dihydro-1H-pyrrol-1-yl)ethyl)amino)-2-oxoethyl)amino)-2-oxoethyl)-3-phenylpropanamide (MIFGG) (product **11**) as yellow solid (308 mg, 96%). ^{1}H NMR (500 MHz, DMSO-d_6, 25 ^{o}C) δ(ppm): 8.74 (t, J = 5.5 Hz, 1H), 8.01 (t, J = 5.9 Hz, 1H), 7.38 – 7.31 (m, 2H), 7.28-7.27 (m, 3H), 7.00 (s, 2H), 4.09 (s, 1H), 3.87 (dd, J = 16.6, 5.6 Hz, 1H), 3.79 (dd, J = 16.7, 5.4 Hz, 1H), 3.68 – 3.59 (m, 2H), 3.47 – 3.41 (m, 2H), 3.21 (dd, J = 12.1, 6.0 Hz, 2H), 3.11 (dd, J = 13.8, 5.0 Hz, 2H).

2. ESI-MS Spectrometry of the Final MIFGG.

ESI-MS spectrometric analyses were performed at the Thermo Finnigan LCQ AD System. The molecular weights of MIFGG were determined to be 402.48 ($+H^+$) (calculated 401.42). The mass spectrometry result indicated that the MIFGG molecule was successfully synthesized.

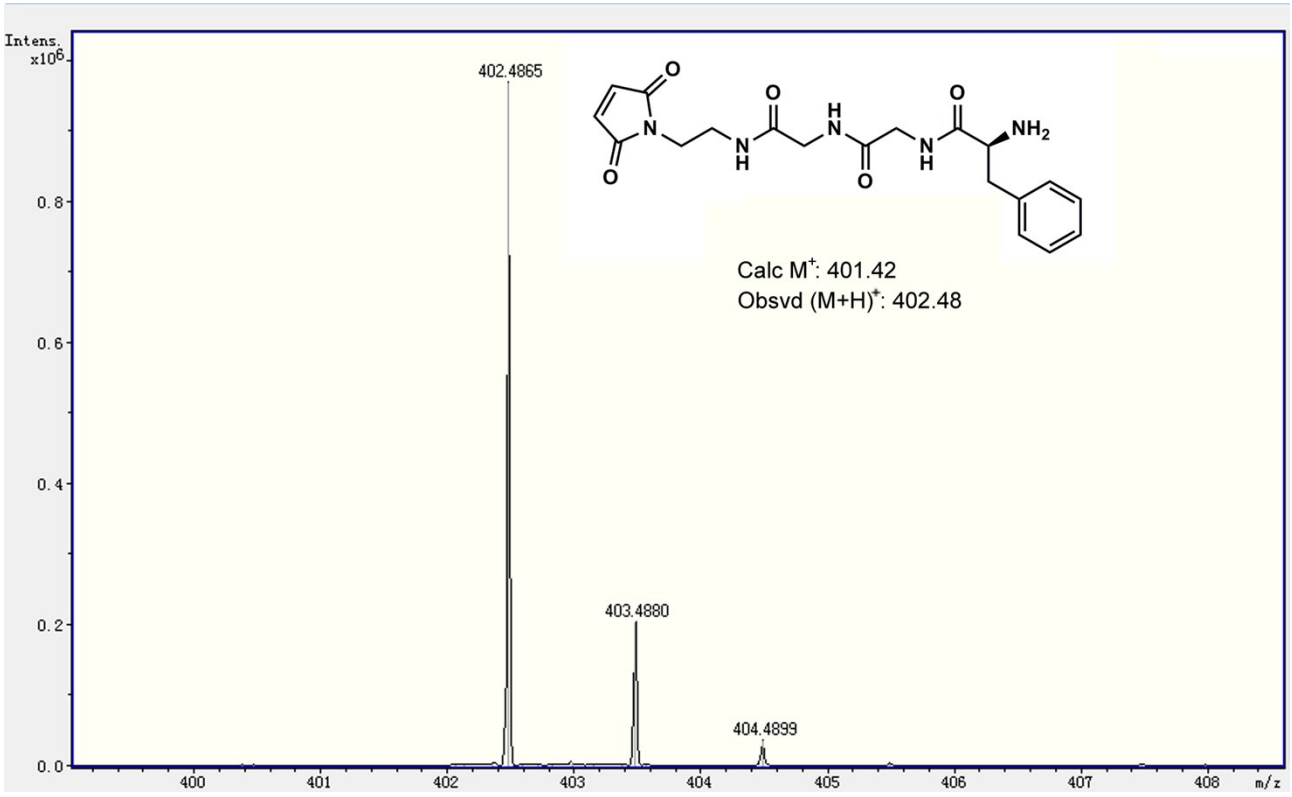

Figure S1. ESI-MS analysis of MIFGG.

3. 13C NMR spectrum of the Final MIFGG.

13C NMR spectroscopy was recorded on a Bruker AVANCE III 500 MHz instrument using D_2O as the solvent.

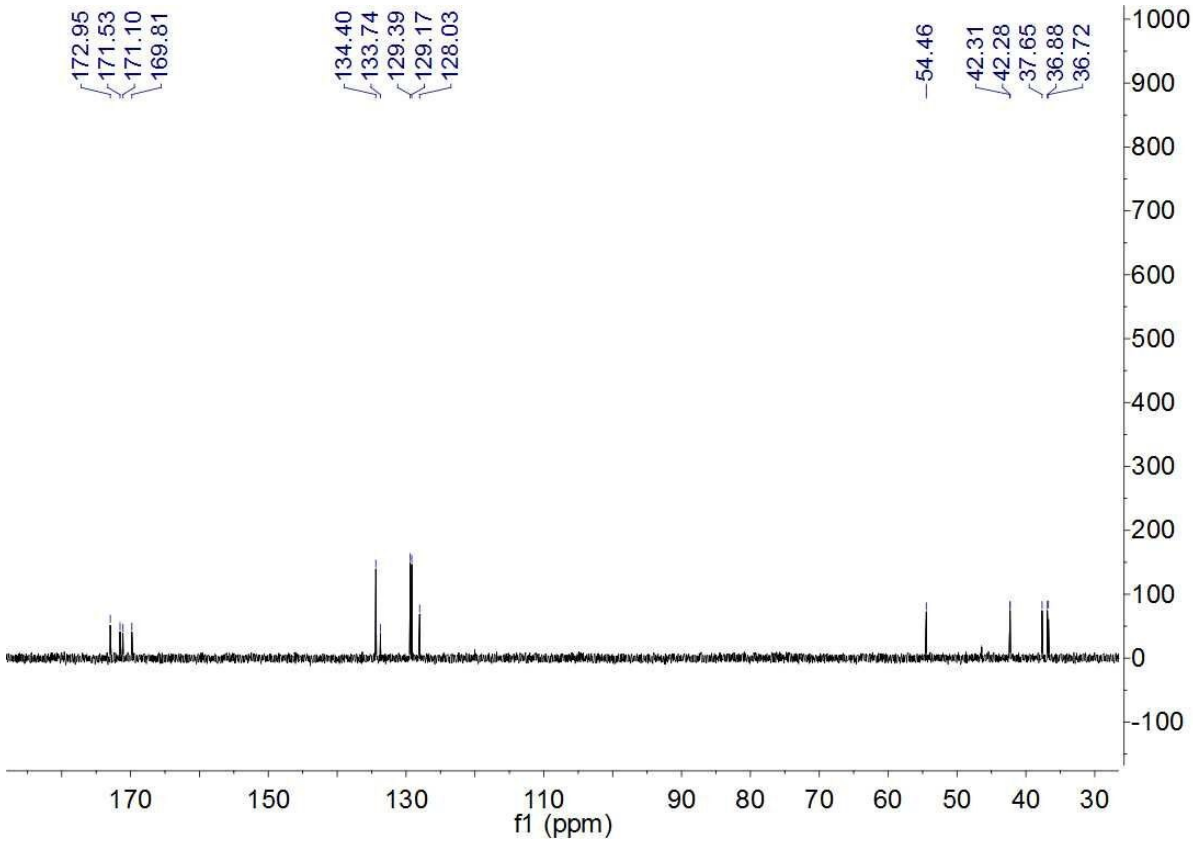

Figure S2. 13C NMR spectrum of MIFGG in D_2O.

4. UV spectrum of the Final MIFGG.

UV-vis absorption spectra was recorded on a Shimadzu 3100 UV-vis-NIR spectrophotometer. λ max(ε)=299 nm (446 $mol^{-1} \cdot dm^3 \cdot cm^{-1}$).

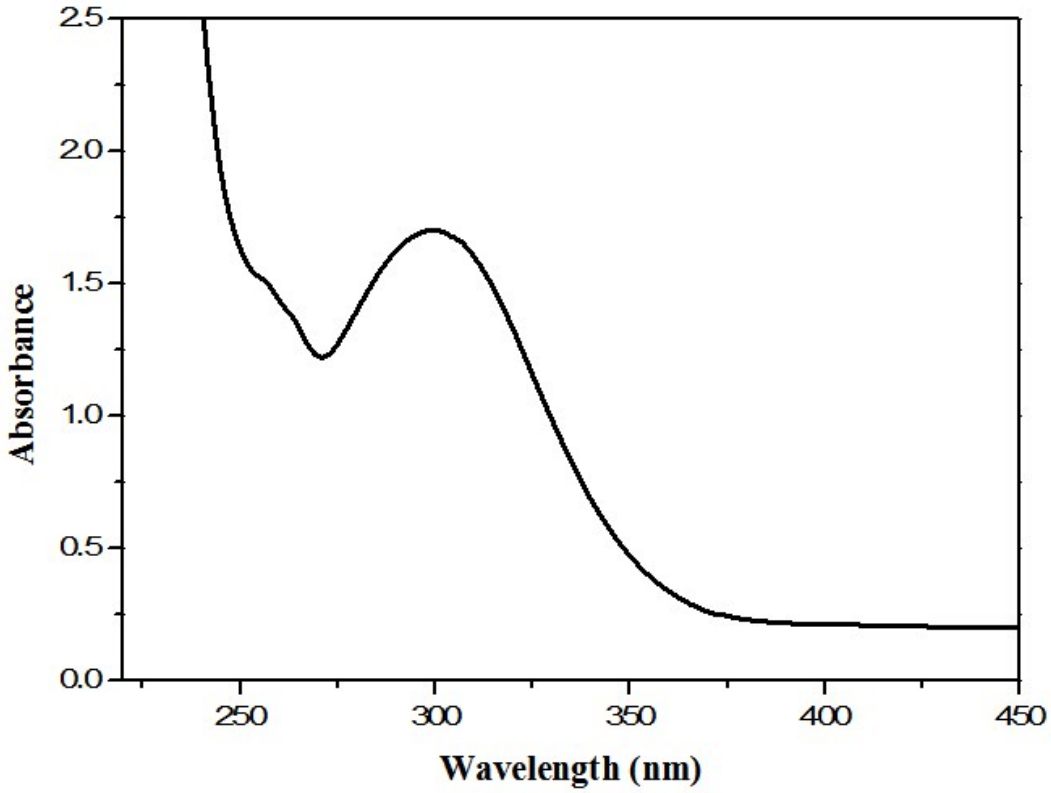

Figure S3. UV spectrum of MIFGG in H_2O.

5. IR spectrum of the Final MIFGG.

IR spectroscopy was recorded on Bruker IFS-FT66V FT-IR spectrometer. IR (cm^{-1}, CaF_2): υ = 3295, 3079, 2942, 1710, 1665, 1546, 1408, 1202, 1170, 1134, 832.

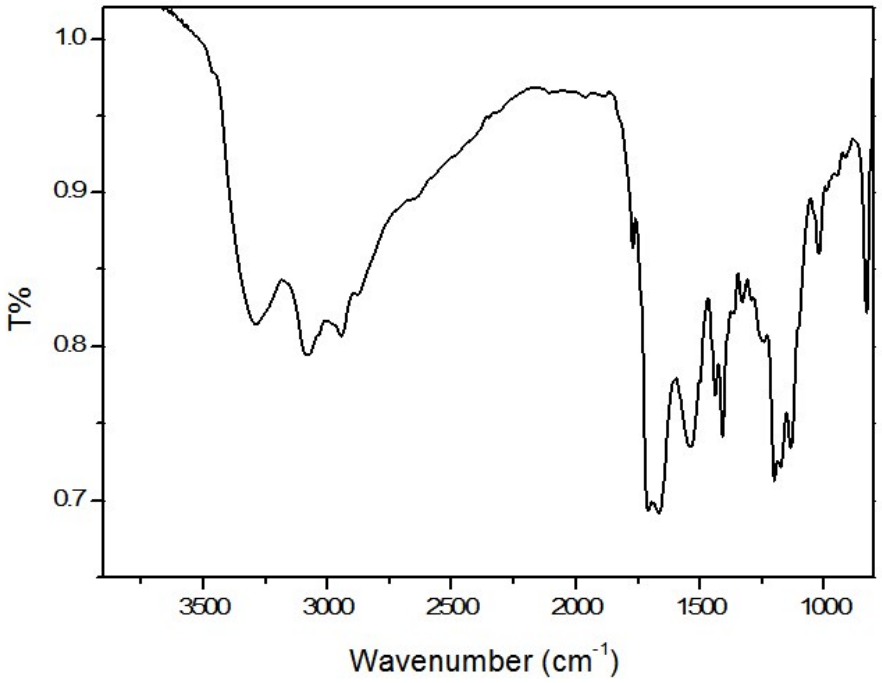

Figure S4. IR spectrum of MIFGG.

6. Site Directed Mutagenesis and Protein Expression/Purification and Modification.

Site directed mutagenesis was carried out on the pGEX-5x-2 plasmid. The mutant plasmid was obtained by PCR site-directed mutagenesis and employing primers were purchased from the Sangon Biotech. Three rounds of mutagenesis were executed to obtain the mutant sjGST 137C (sjGST_C84S _C168S_C177S). The resulting plasmids were transformed into DH5α E. coli cells. Sequencing of the mutant plasmid was performed at the Sangon Biotech.

The protein was then purified by Glutathione Sepharose 4B (Glutathione Sepharose 4B is designed for the rapid, single-step purification of glutathione S-transferses). Excessive glutathione was removed by dialysis. The purified sjGST 137C was concentrated with freezedrying equipment. The resulting protein powder was dissolved in 20 mM Tris-HCL buffer (pH=7.4) to a concentration of 1 mM, and react with ten-fold of MIFGG with stirring overnight at 4 ^{o}C. The resulting solution was centrifuged to remove denatured proteins and excess MIFGG was removed by rapid gel filtration with a Sephadex G-25 column. The purity of the final sjGST-2FGG was determined by SDS-PAGE gel electrophoresis (Figure S5).

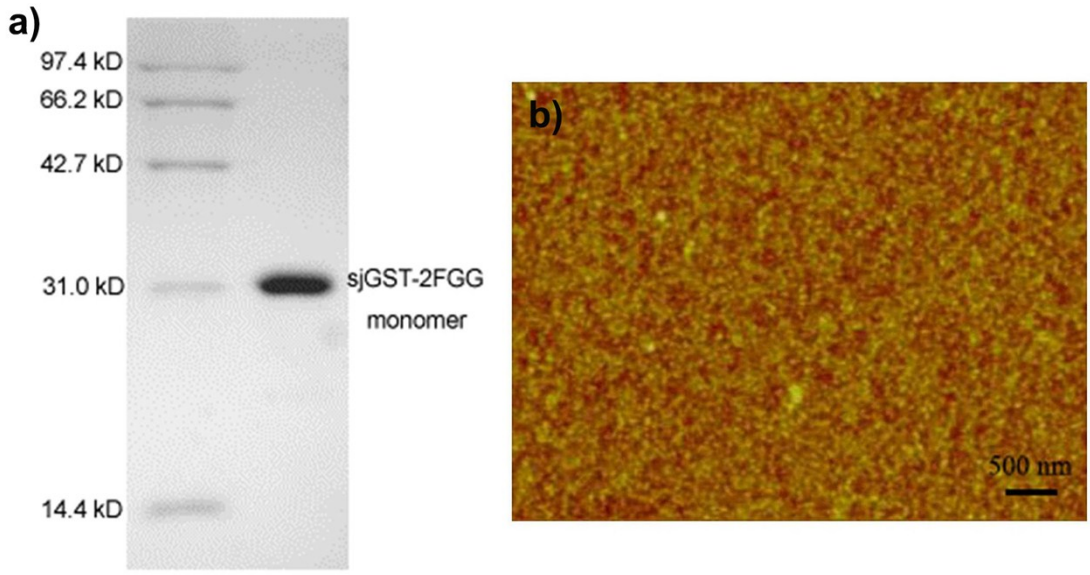

Figure S5. a) SDS-PAGE analysis of sjGST-2FGG, Lane1: marker proteins; lane 2: the monomer of sjGST-2FGG. b) AFM characterization of sjGST-2FGG.

7. MALDI-TOF Mass Spectrometry of sjGST 137C and sjGST-2FGG.

MALDI-TOF mass spectrometry was performed using autoflex speed^{TM} TOF/TOF mass spectrometer (Bruker, daltonics Inc., USA) as described[3]. Prior to determination, all the samples were desalted by dialysis against MilliQ water with dialyzing tubes, Slide-A-Lyzer Dialysis Cassettes (Pierce) or G25 filtration. The resulting GST derivatives were lyophilized and resolved at a concentration of 10 μM. For preparation, sinapic acid was chosen as matrix which was saturated in 70% acetonitrile and supplemented with 1% trifluoroacetic acid. 1 μl samples and 1 μl matrix were sequentially dropped onto the ground steel and dried in air. The molecular weight of sjGST 137C was determined to be 27872 Da (calculated 27871 Da). Molecular weight of sjGST-2FGG was determined to be 28274 Da (calculated 28272 Da), which was in close agreement with the theoretical value. The mass spectrometry result indicated that the MIFGG molecules were successfully linked onto sjGST 137C surfaces.

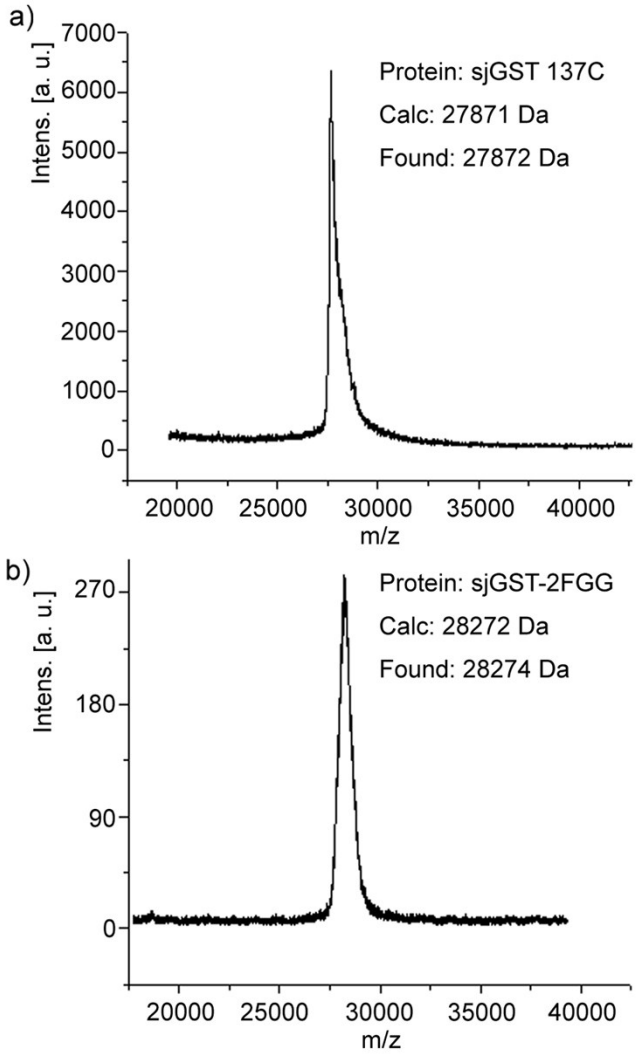

Figure S6. MALDI-TOF mass spectrometry analysis of (a) sjGST-137C and (b) sjGST-2FGG.

8. DLS investigation of sjGST-2FGG self-assembly with time.

DLS was performed to study the hydrodynamic diameters of GST-2FGG-CB[8] self-assemblies varying with time. The GST-2FGG was dissolved in 20 mM pH=7.0 PBS to a concentration of 10 μM, and react with equivalent CB[8]. The hydrodynamic diameters of the self-assemblies increase with time, which also confirmed the bottom-up self-assembly mode (Figure S7).

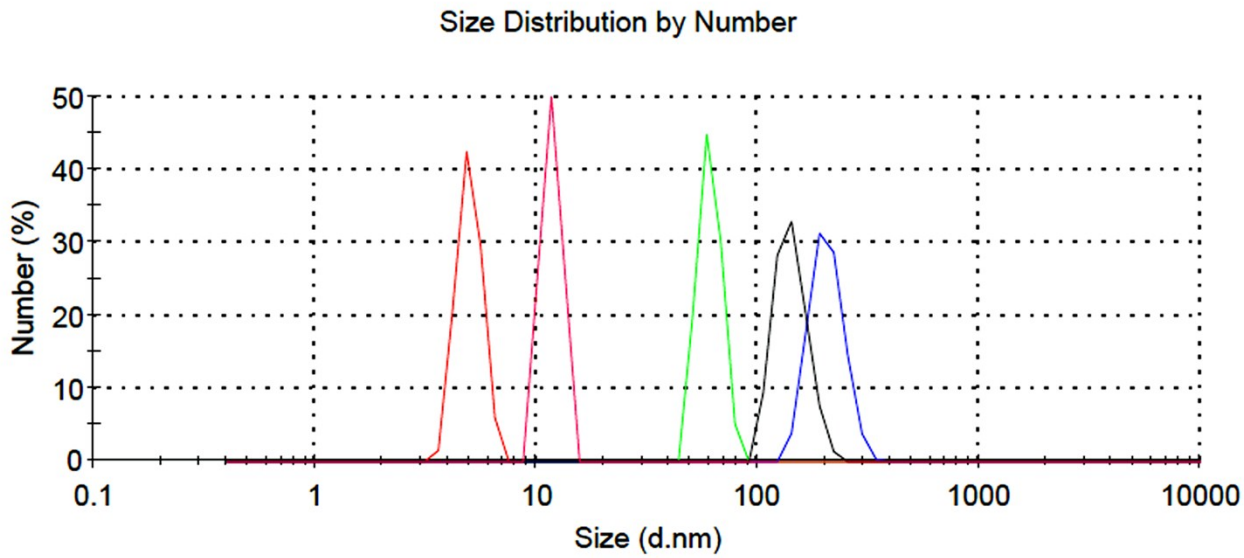

Figure S7. The dynamic light scattering (DLS) analysis of the hydrodynamic diameters of sjGST-2FGG before the addition of CB[8] (red trace), and the self-assemblies after the addition of CB[8] at 10 mins (light pink trace), 30 mins (green trace), 45 mins (black trace), 60 mins (blue trace).

9. Investigation of the relative position of two sjGST-2FGG linked with CB [8].

The MIFGG molecule structure was constructed and optimized with GaussView. The visualization of cartoon representations and the docking of two sjGST-2FGG molecule were performed by PYMOL program. As shown in Figure S8, compared with metal coordination motif, the MIFGG molecule is relatively long and flexible. In addition, the mean diameter of the internal cavity of CB[8] can reach to ~8.8 Å[4], which will eliminate the protein surface interactions. Thus this self-assemblies are mainly dictated by strong host-guest interactions and we turn to the ring-chain competition mechanism for the construction of ordered protein superstructures.

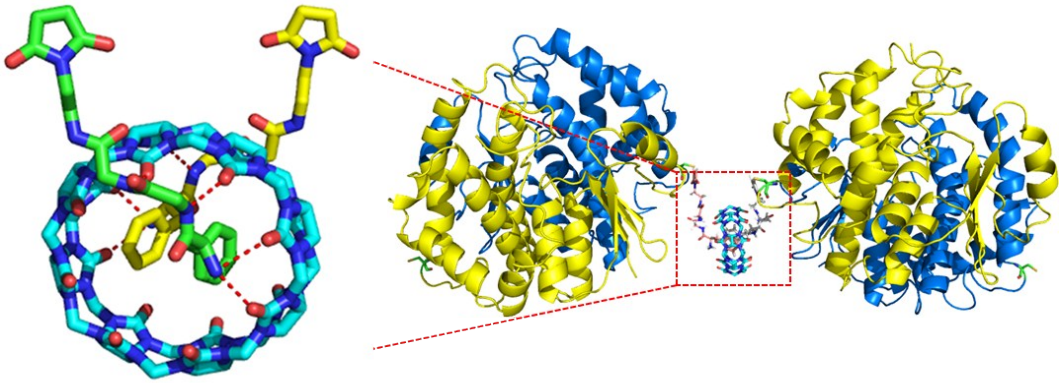

Figure S8. Cartoon representation of two protein building blocks bound with MIFGG-CB[8] interactions. Enlarged: Detailed interactions between two MIFGGs and CB[8][5].

10. Labeling of sjGST-2FGG with FITC.

FITC was dissolved in dimethyl sulfoxide (DMSO) to a concentration of 1 mg/ml and added to the protein solution (2 mg/ml) in 0.1 M sodium carbonate buffer (pH=9) at a ratio of 50 µl of FITC solution per 1 ml protein solution. The reaction was incubated in the dark for 8 hours at 4 °C and subsequently quenched by the addition of NH_4Cl to a final concentration of 50 mM. The resulting solution was centrifuged to remove denatured proteins and excess FITC was removed by dialysis.

11. TEM investigation of sjGST-2FGG self-assembly with 1 equiv of CB[8] at low concentration.

Transmission electron microscopy (TEM) measurements were performed using a JEM-2100F transmission electron microscope with 200 kV accelerating voltage. A 5 μl aliquot of sjGST-2FGG (0.32 μM) self-assembly with 1 equiv of CB[8] formed in 20 mM PBS (pH=7.0) buffer was deposited on the copper grids for 5 min, rinsed twice with pure water, and then negatively stained with 1% sodium phosphotungstate prior to TEM detection. As shown in Figure S9a, protein nanorings as well as small spiral-like structures were obtained. Interestingly, a‘bracken’-like spiral structure with relatively long tail was also captured (Figure S9b). From nanorings, nanospirals, nanospirals with long tails to protein nanowires, we assume this spiral-like structure is the intermediate product of nanoring-nanowire transition.

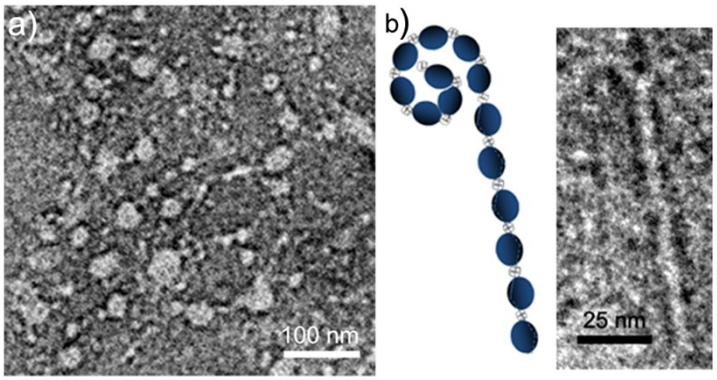

Figure S9. TEM characterization of sjGST-2FGG self-assembly with 1 equiv of CB[8] at low concentration. a) protein nanorings and b) nanospiral with a relatively long tail can be observed.

12. Suggested Mechanism of the 'Nanospiral' Formation

As shown in Figure S10, considering the supramolecular nature of host-guest interactions, the CB[8]/FGG binding pair can undergo a dynamic equilibrium between association and dissociation, which renders the equilibrium between nanorings and 'gapped nanorings'. We assumed that if the local concentration is high enough, more free building blocks can associate with the available end of the gapped nanorings and form into nanospirals, whose 'tail' can continuously grow and finally extend into nanowires.

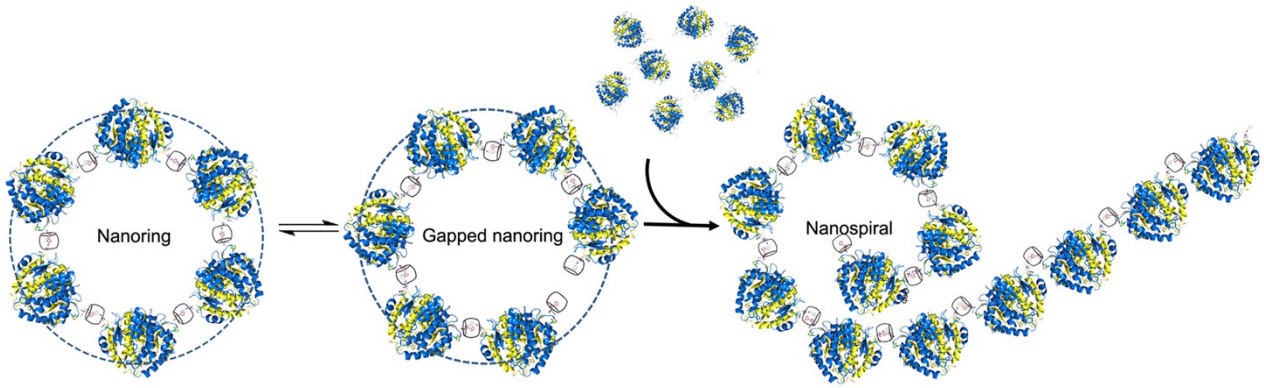

Figure S10. Suggested mechanism for the 'nanospiral' formation.

13. TEM investigation of sjGST-2FGG self-assembly with 1 equiv of CB[8] at high concentration.

Transmission electron microscopy (TEM) measurements were performed using a JEM-2100F transmission electron microscope with 200 kV accelerating voltage. A 5 μl aliquot of sjGST-2FGG (3.2 μM) self-assembly with 1 equiv of CB[8] formed in 20 mM PBS (pH =7.0) buffer was deposited on the copper grids for 5 min, rinsed twice with pure water, and then negatively stained with 1% sodium phosphotungstate prior to TEM detection. As shown in Figure S11, entangled protein nanowires can be clearly observed.

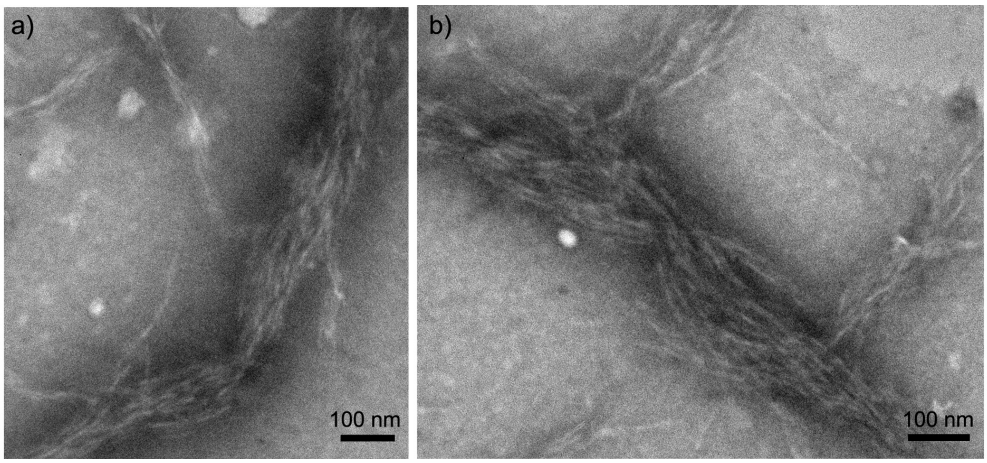

Figure S11. a), b) TEM images of entangled protein nanowires formed at high protein concentration.

14. Characterization of nanoring/nanowire coexistence when assembled at high concentration.

As suggested by the typical ring-chain competition mechanism[6], above the critical concentration, the equilibrium concentration of the linear structures will increase with the protein concentration. However, the equilibrium concentration of ring structures remains still, which means protein nanorings and protein nanowires can coexist when assemble at high protein concentrations (Figure S12a). This phenomenon can be observed in our self-assembly system, as shown in Figure S12b, S12c, ring-like structures can be discerned among the bundled nanowires in AFM and TEM images. This observation further confirmed that the constructed protein self-assembly system obey the typical ring-chain competition mechanism.

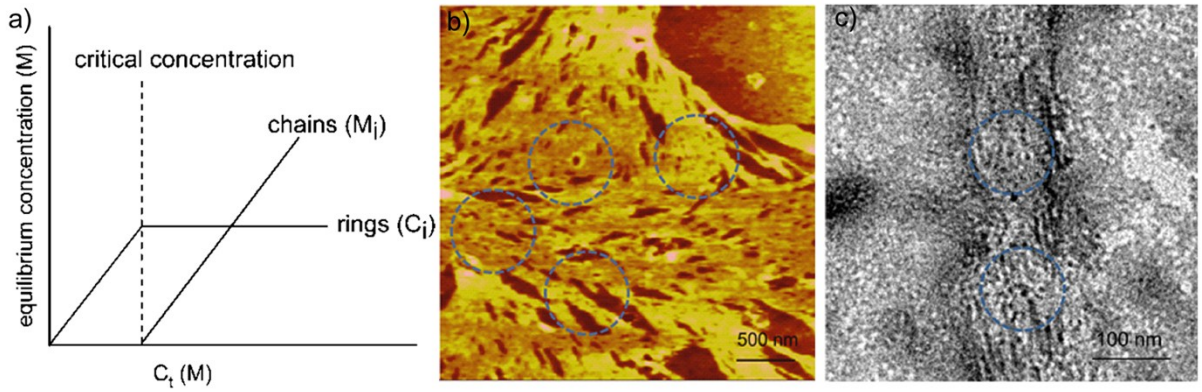

Figure S12. a) The relationship between the equilibrium concentration of chains and rings in a ring-chain competition supramolecular polymerization[6]. b) AFM characterization c) TEM characterization of bundled protein nanowires among which ring-like structures can be discerned.

15. Morphological characterization of sjGST-2FGG assemblies after re-equilibrium induced by dialysis.

SjGST-2FGG formed into disordered aggregates when self-assembled with excess CB[8] at high concentration, the mixture was treated with dialysis to induce re-equilibrium, after which the resulting sample was morphologically characterized by AFM and TEM . As shown in Figure S13, evenly dispersed single protein nanowires can be observed both with AFM and TEM images. Moreover, single protein nanowires can further assemble into superwires with greater rigidity and stability (Figure 7, Figure S13e).

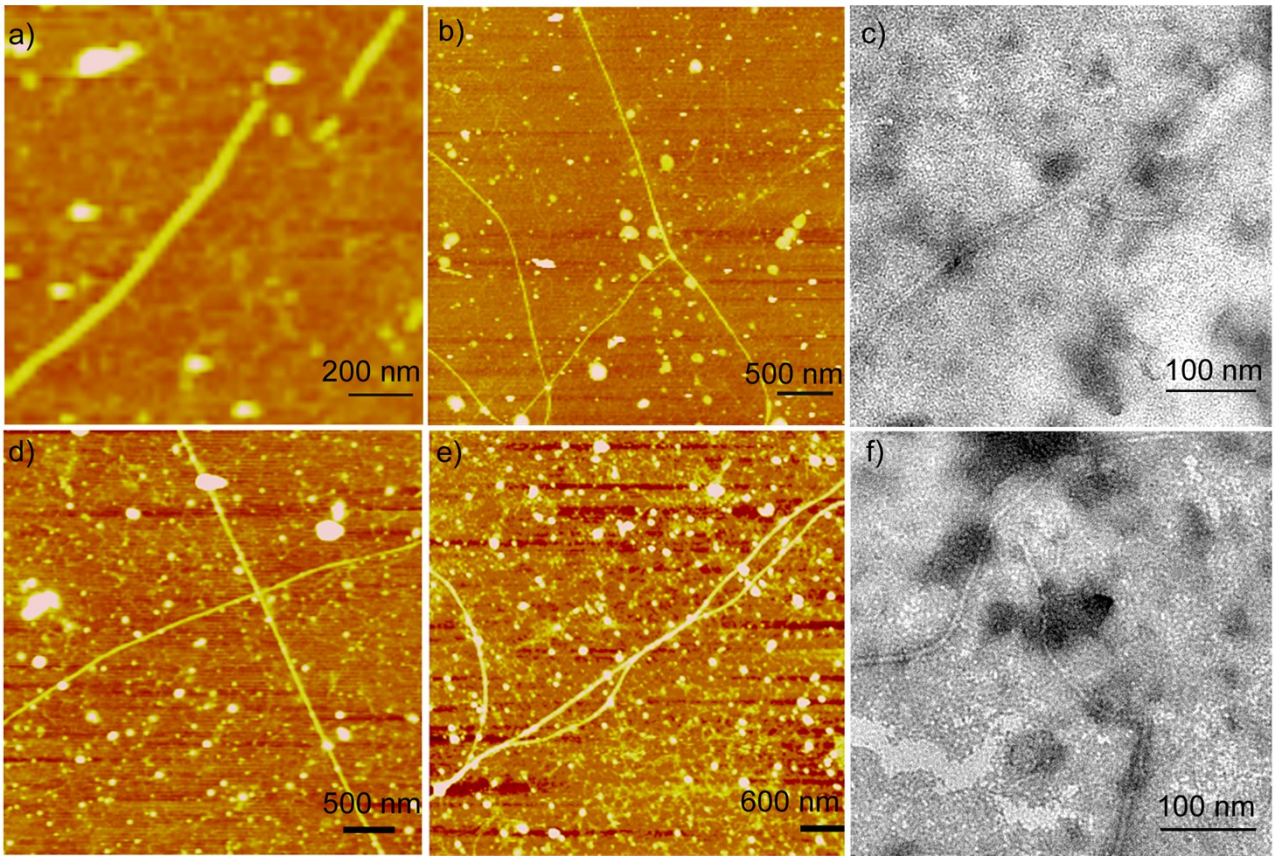

Figure S13. Morphology characterization of the resulting mixture after treating disordered aggregates, which formed with excess CB[8] at high sjGST-2FGG concentration, with dialysis. a), b), d), e) AFM height image of sjGST-2FGG assemblies, in which evenly dispersed protein nanowires can be observed. c), f) TEM images also indicate the formation of protein nanowires.

16. Electrical field characterization of sjGST Surface.

To investigate the interactions between protein nanowires, we probed the electrical field of sjGST surface. Follow the designed position 137 that linked with MIFGG as an axis, when rotated the structure, a side surface (Figure S14a) abundant with negative charges and two side surfaces rich in positive charges can be identified. (Figure S14b, S14c). The electrical interactions between the side surfaces may attribute to the formation of multiple protein superwires.

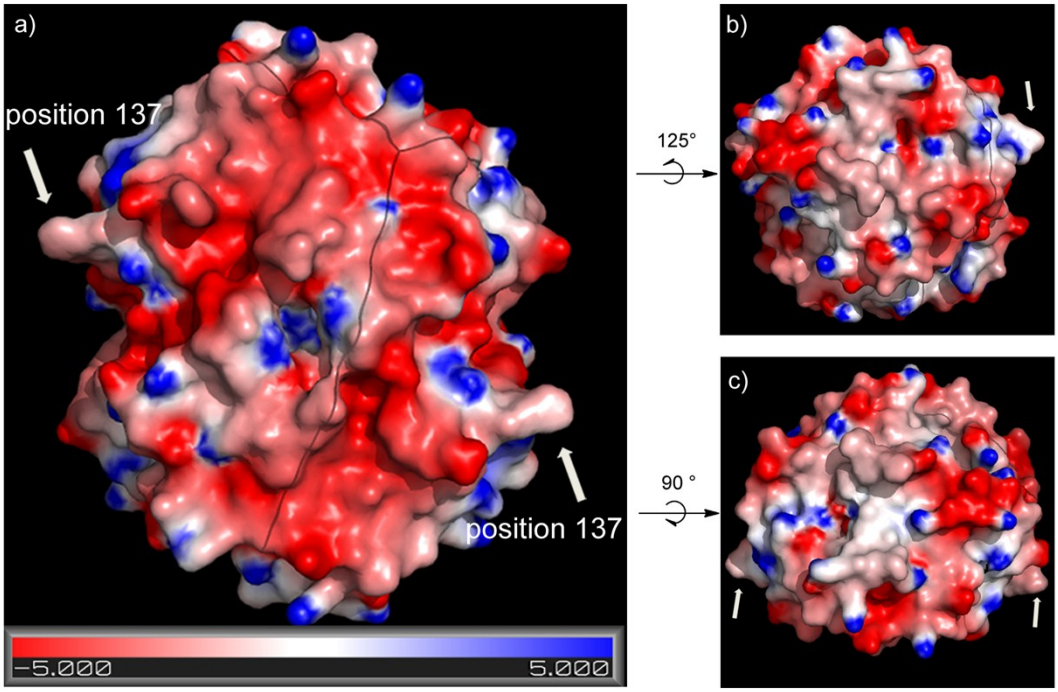

Figure S14. Surface electrical field of sjGST. Our designed position 137 was indicated with white arrows. The red color is for negative charges, and blue color is for positive charges. (a) Side view of the sjGST dimer structure, from this angle, a surface with vastly distributed negative charges can be identified. (b) Rotating the structure upward to find a surface rich in positive charges (c) Rotating the structure downward, another surface rich in positive charges can be identified.

References for Supporting Information

[1] G. Mantovani, F. Lecolley, L. Tao, D. M. Haddleton, J. Clerx, J. J. Cornelissen and K. Velonia, *J. Am. Chem. Soc.,* 2005, **127**, 2966-2973.

[2] W. S. Saari, J. E. Schwering, P. A. Lyle, S. J. Smith and E. L. Engelhardt, *J. Med. Chem.,* 1990**,** **33**, 97-101.

[3] M. E. Bush, N. D. Bouley and A. R. Urbach, *J. Am. Chem. Soc*., 2005, **127**, 14511-14517.

[4] J. W. Lee, S. Samal, N. Selvapalam, H.-J. J. Kim and K. Kim, *Acc. Chem. Res.,* 2003, **36**, 621–630.

[5] L. M. Heitmann, A. B. Taylor, P. J. Hart and A. R. Urbach, *J. Am. Chem. Soc.,* 2006, **128**, 12574–12581.

[6] T. F. A. D. Greef, M. M. J. Smulders, M. Wolffs, A. P. H. J. Schenning, R. P. Sijbesma and E. W. Meijer, *Chem. Rew.,* 2009, **109**, 5687–5754.